A Continuously Variable Coaxial-Line Attenuator

EDWARD G. CRISTAL, FELLOW, IEEE

Abstract—**This paper reports on a new continuously variable coaxial-line attenuator that utilizes a center conductor of semi-insulating material. Some general design details and data are given. Specific design details for an octave bandwidth prototype attenuator are presented and discussed, and experimental results for the prototype are given. The theory on which the attenuator is based is developed and several interesting theoretical results are described.**

INTRODUCTION

THIS PAPER reports on a new continuously variable coaxial-line attenuator that utilizes a center conductor of semi-insulating material. Principle features of the attenuator are:

1) attenuation proportional to attenuator length;
2) moderate to small input and output VSWR;
3) low insertion loss in the minimum attenuation position;
4) dynamic range limited only by the permissible physical length of the attenuator;
5) transmission phase proportional to length and approximately proportional to frequency;
6) frequency dependent attenuation, but that which can be minimized by proper design.

A somewhat simplified longitudinal sectional view of the coaxial-line attenuator is given in Fig. 1. The key components of the design are Items 1–7. Items 1 and 2 constitute a coaxial line which is fixed in position and made from conventional metals. Items 3 and 4 constitute a coaxial line which is movable and also made from conventional metals. (The situation can be reversed with 1 and 2 movable and 3 and 4 fixed.) Items 5 and 6 are thin dielectric beads used for alignment and support of the coaxial-line center conductors. Item 7 is a center conductor concentric with 4 and 2, bonded to 4, and made of single crystal or amorphous semi-insulating material. An important refinement in the design, not illustrated in Fig. 1, is a thin skin of lossy material on the outer conductor of Item 1. The lossy material absorbs RF energy propagating between conductors 1 and 3 and further serves to maintain a constant impedance at the reference plane of the support beads 5.

A qualitative description of the attenuator's operation follows. Assume coaxial line 3–4 is movable, coaxial line 1–2 is fixed, and RF energy is propagating from coaxial line 3–4 to 1–2. For minimum attenuation coaxial line

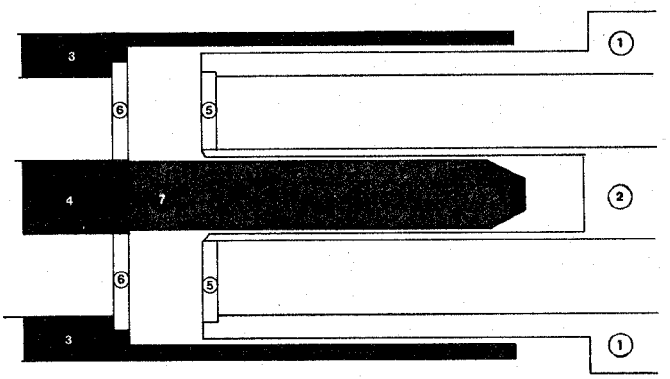

Fig. 1. A continuously variable microwave coaxial attenuator, longitudinal section view.

3–4 is moved to a position in which beads 5 and 6 are nearly touching. In this position the semi-insulating material 7 is almost entirely covered by center conductor 2. RF energy propagating from coaxial line 3–4 is transmitted to line 1–2 with small losses due to mismatch at the dielectric beads 5 and 6, and coupling to the circular transmission line formed by 1 and 3. (Measurements on experimental models operating to 13 GHz showed maximum losses under 0.75 dB.) As coaxial line 3–4 is moved to the left, the semi-insulating material 7 is exposed and a coaxial line is formed between 3 and 7. RF energy, propagating in the TEM mode in line 3–4, launches a TM-01 mode wave with complex propagation constant in coaxial line 3–7, where it is attenuated and phase shifted. At the interface of lines 3–7 and 1–2 the TM-01 mode launches a TEM wave in coaxial line 1–2. RF currents propagating in the semi-insulating material 7 are capacitively coupled to line 2[1], and this coupling is enhanced by the fact that the interior of line 2 together with material 7 forms a lossy, essentially cutoff, circular waveguide. At the onset of attenuation, as line 3–4 is moved away from its minimum-attenuation position, the attenuation versus position relationship is slightly nonlinear due to circuit interactions. However, within a few millimeters of extension the attenuation characteristic becomes linear and remains so thereafter. The maximum attenuation is determined by the allowable displacement of line 3–4 from line 1–2.

Gunn and Hogarth [1] have also reported using a semi-insulator to achieve a variable attenuator. Their concept,

Manuscript received January 15, 1979; revised October 15, 1979.

The author is with the Hewlett-Packard Company, Palo Alto, CA 94304.

[1]In theory the currents are conductively coupled, but in practice an insulating layer is formed on the semi-insulator surface.

0018-9480/80/0300-0191$00.75 ©1980 IEEE

much different than reported here, utilized a TE-10 waveguide in which a germanium slab was set at an acute angle across the guide. The attenuation was varied by modifying the conductivity of the semi-insulator using a pulsed control current.

The attenuator described here perhaps has some physical similarities to other coaxial-line attenuators [2]–[4]. However, its mechanics and its attenuation principles are unique. The center conductor of the present device is, and is required to be, a bulk single crystal or amorphous semi-insulating material extending from zero radius to its outer limit. Other devices typically use thin films of lossy carbon, carbon-like, polyiron, etc., amorphous materials deposited on a nonconducting center conductor, or in some cases the outer conductor. In these cases the thin-film thickness is less than a skin depth in order to achieve attenuation frequency independence; the propagation mode is basically TEM. The present device uses a composite TM-01 mode in which the entire bulk of the semi-insulating material contributes to the attenuation. The magnitude of the current is nonnegligible throughout the semi-insulator.

Theory

The generic form for the lossy part of the attenuator is shown in Fig. 2. It is basically a conventional coaxial line in which the metallic center conductor has been replaced by a semi-insulating material. The wave mechanism is a *composite* TM-01 mode in which the propagation constant is complex, and the fields extend significantly into the semi-insulating material. In the composite TM-01 mode there are two components of electric field and one component of magnetic field: E_r, E_z, and H_θ. All components are independent of θ. In the conventional TM-01 modes of coaxial lines and circular waveguides E_r and H_θ are orthogonal in time. However, in the composite TM-01 mode described herein E_r and H_θ are generally nonorthogonal in time in both Regions I and II.

For design purposes the key parameters required are the complex propagation constant and complex characteristic impedance as a function of geometry and electromagnetic constants of the semi-insulator. Theoretically, this requires a rigorous solution of Maxwell's equations within Regions I and II. To this end we define the following parameters:

- ϵ_0 free space permittivity (8.854 pF/m).
- ϵ permittivity of Region II.
- μ_0 free-space permeability ($4\pi \times 10^{-7}$H/m).
- μ permeability of Region II.
- σ conductivity of Region II (mhos/m).
- ω radian frequency.
- ρ a/b (a and b given in Fig. 2).
- J_0 Bessel function of the first kind of order zero.
- J_1 Bessel function of the first kind of order one.
- N_0 Bessel function of the second kind of order zero.
- N_1 Bessel function of the second kind of order one

propagation in z direction given by $\exp(-\Gamma z)$.

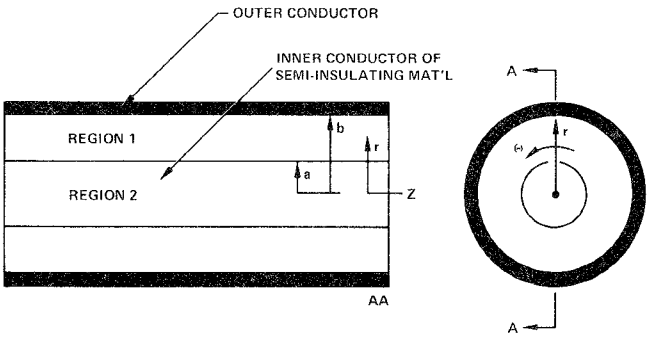

Fig. 2. Generic form of coaxial-line attenuator.

- Γ $\alpha + j\beta$ where α is the attenuation, in nepers/meter, and β is the transmission phase, in radians/meter.
- $\hat{\gamma}$ $SQRT\ [\Gamma^2 - (\sigma + j\omega\epsilon)(j\omega\mu)]$ = the propagation constant in the r direction in Region II.
- γ $SQRT[\Gamma^2 - (j\omega\epsilon_0)(j\omega\mu_0)]$ = the propagation constant in the r direction in Region I.
- z (γb).
- W $(\hat{\gamma}a/\rho)(j\omega\epsilon_0/(\sigma + j\omega\epsilon))(J_0(\hat{\gamma}a)/J_1(\hat{\gamma}a))|$.
- $F(z)$ $[(J_0(\rho z)N_0(z) - N_0(\rho z)J_0(z))/(J_1(\rho z)N_0(z) - N_1(\rho z)J_0(z))]$.

The field expressions are given in the Appendix with the normalized low-frequency current I as a multiplicative constant. The tangential components of the fields in Regions I and II must be continuous at the interface $r = a$ [5]. In terms of the above definitions this yields the complex transcendental equation

$$zF(z) = W. \tag{1}$$

The solution to (1) yields Γ and subsequently by back substitution all of the field components in Regions I and II.

Equation (1) was solved on a digital computer for a range of electromagnetic parameters for several commercially available materials. Two numerical methods, the details of which are too lengthy to include in this paper, were used to solve (1).

1) Newton's method applied to (1), yielding the iterative complex equation

$$z_{i+1} = \frac{W - z_i F(z_i)}{F(z_i) + z_i F'(z_i)} + z_i \tag{2}$$

where F' is the derivative of F with respect to z.

2) A minimization procedure: The procedures were mixed dynamically in a single computer program so that solutions could be found in minimum time without operator interaction. Both methods were found necessary as Newton's method did not converge over the entire range of Γ. On the HP3000 computer it took less than a few seconds per solution.

Characteristic Impedance

Because the mode is not TEM there is the usual ambiguity in the definition of the characteristic impedance.

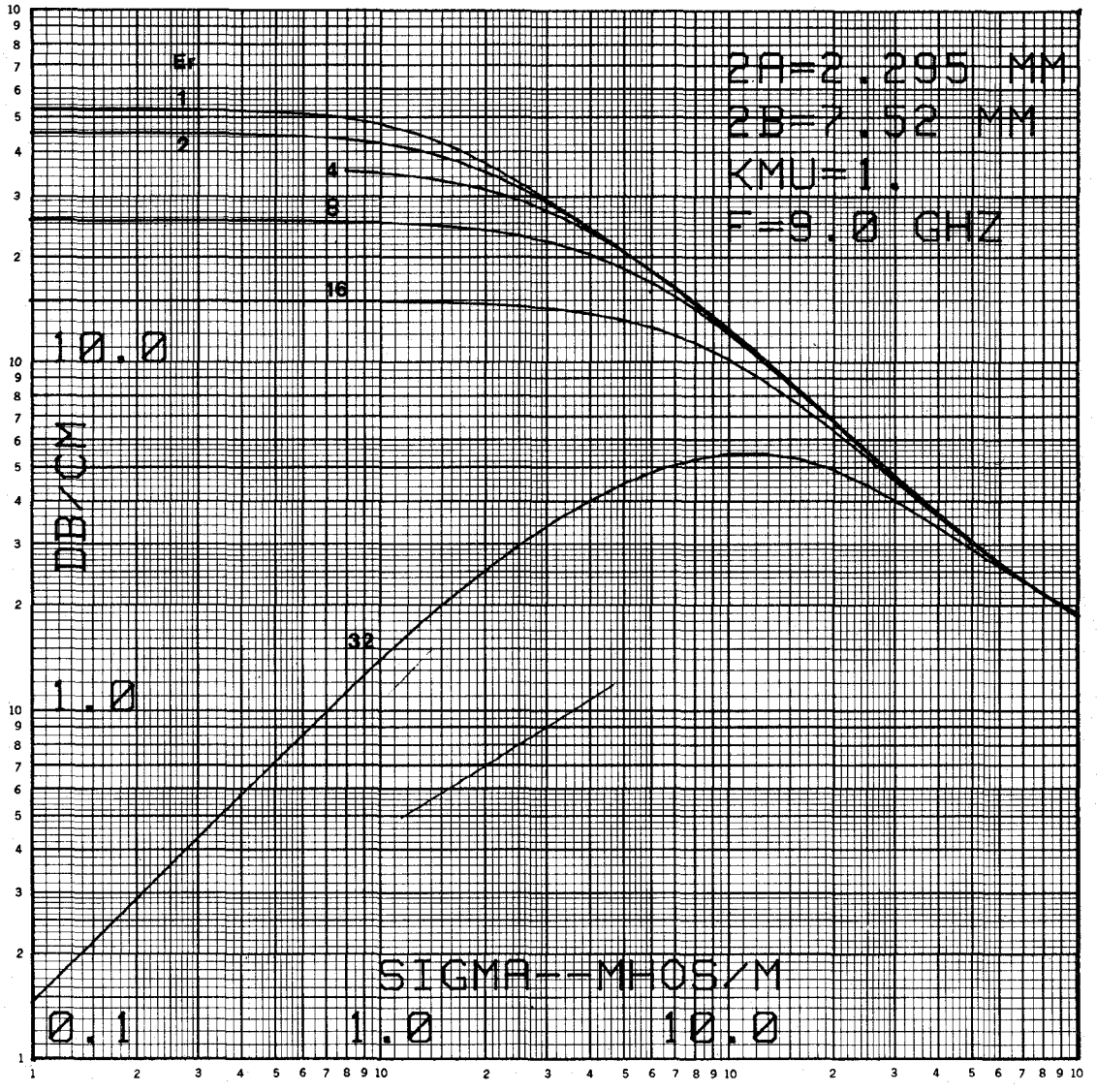

Fig. 3. Theoretical attenuation slope versus conductivity.

In this work the characteristic impedance was defined on a power-voltage basis according to the equation

$$P+jQ=\tfrac{1}{2}\iint \boldsymbol{E}^*\times\boldsymbol{H}\cdot d\boldsymbol{A}=\tfrac{1}{2}\frac{|V|^2}{Z_0} \tag{3}$$

where the integration on the left-hand side of (3) extends over Regions I and II, V is the voltage from $r=0$ to $r=b$, Z_0 is the complex characteristic impedance, and P and Q are the real and reactive powers, respectively. Substituting the appropriate field expressions given in the Appendix into (3), solving for Z_0 yields after simplification

$$Z_0=\frac{1}{2\pi}\frac{\left|Z_{w_{II}}\int_0^a H_{\theta_{II}}\,dr+Z_{w_I}\int_a^b H_{\theta_I}\,dr\right|^2}{Z_{w_{II}}^*\int_0^a r|H_{\theta_{II}}|^2\,dr+Z_{w_I}^*\int_a^b r|H_{\theta_I}|^2\,dr} \tag{4}$$

where H_{θ_I} and $H_{\theta_{II}}$ are given in the Appendix, $Z_{w_I}=\dfrac{\Gamma}{j\omega\epsilon_0}$, $Z_{w_{II}}=\dfrac{\Gamma}{\sigma+j\omega\epsilon}$, and the superscript * indicates complex conjugate.

Theoretical Results

Shown in Figs. 3–6 are some particularly interesting results of the theoretical analysis. All data are for a coaxial line having an inner diameter of 2.295 mm and outer diameter of 7.52 mm. The relative permeability of the line is 1 and the frequency is 9.0 GHz. The curves are plotted as a function of conductivity of Region II (the semi insulator) with the relative permittivity of Region II as a parameter. The relative permittivity varies from 1 to 32 in a binary sequence. Since for $\epsilon_r=32$, $\omega\epsilon=16.0$ at 9.0 GHz, the conductivity range was terminated at $\sigma=100$ mhos/m. Above this value of conductivity the inner conductor is primarily metallic and no particularly useful information for this investigation was apparent. The conductivity of the outer conductor was made infinite in the calculations.

Fig. 3 presents attenuation in decibels/centimeter and is of particular theoretical interest because it shows for the first time a continuous transition from a conventional coaxial line operating in what is normally considered the

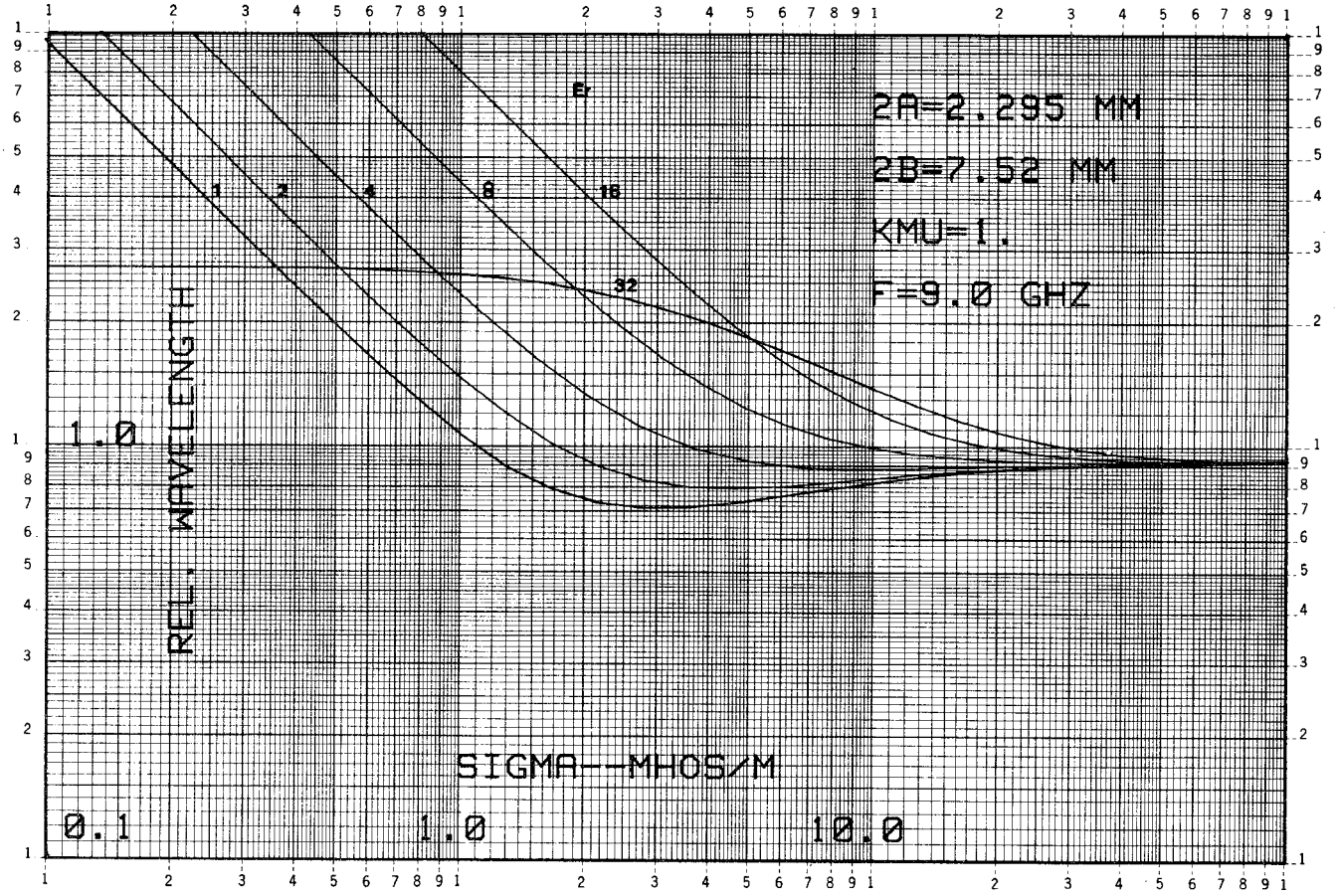

Fig. 4. Theoretical normalized guide wavelength versus conductivity.

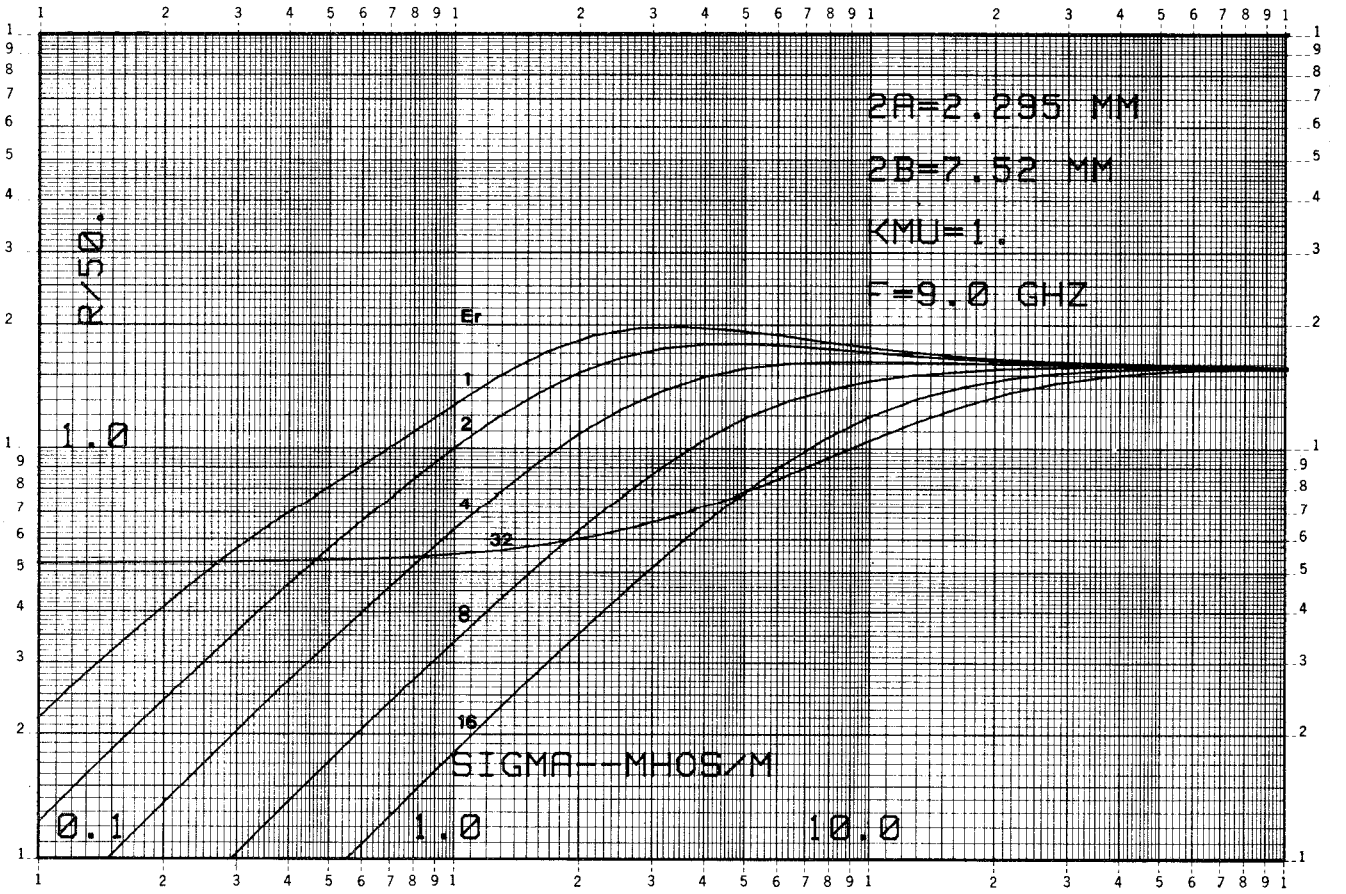

Fig. 5. Theoretical normalized real part characteristic impedance versus conductivity.

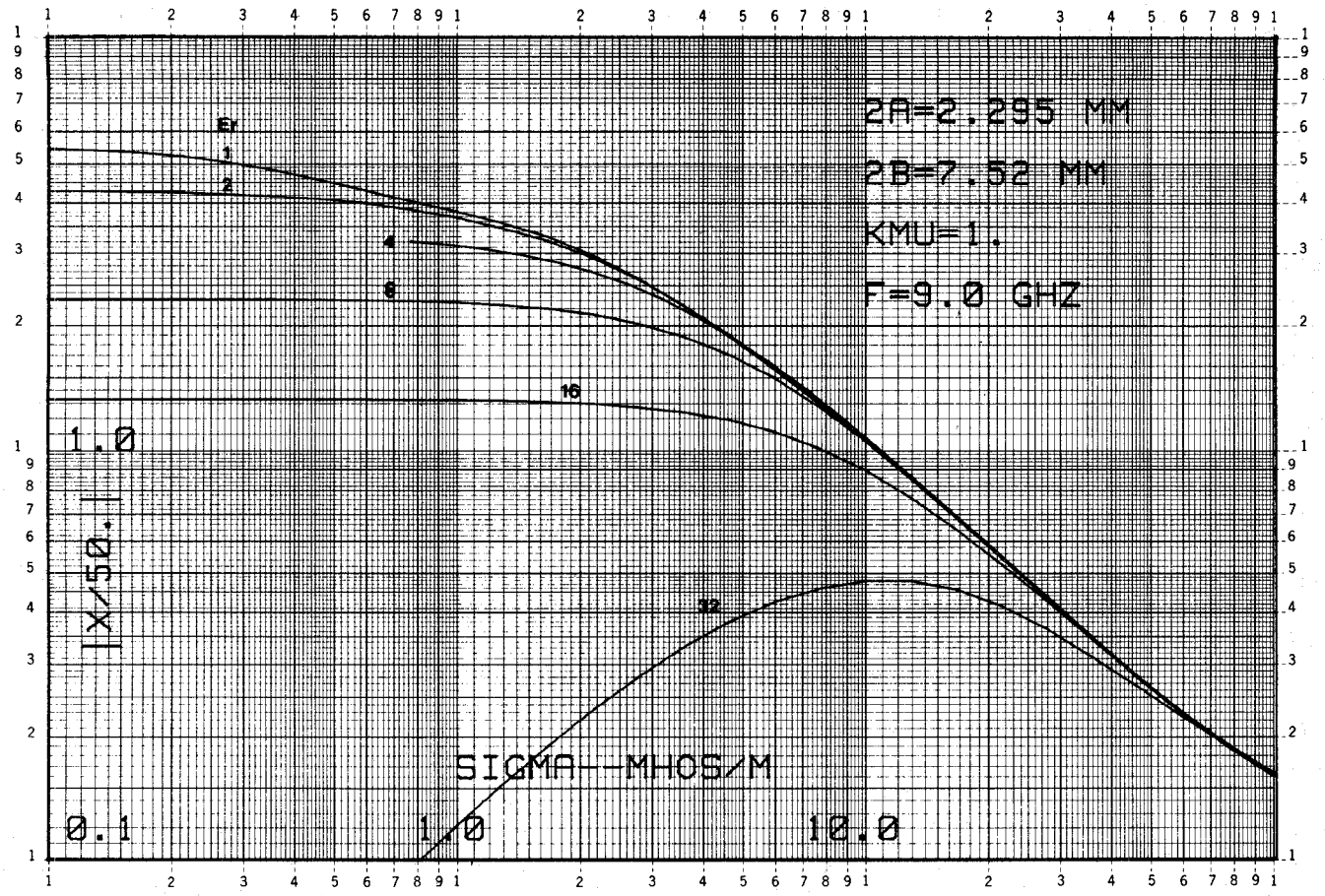

Fig. 6. Theoretical normalized imaginary part characteristic impedance versus conductivity.

TEM mode into a circular waveguide TM-01 mode. More explicitly, the regions of high conductivity in Figs. 3–6 correspond to coaxial lines with metallic center conductors, while the regions of low conductivity correspond to circular waveguides loaded with concentric dielectric cylinders having relative dielectric constants of from 1 to 32. For example, in the case of $\epsilon_r = 1$, corresponding to an idealized circular waveguide of diameter 7.52 mm, the theoretical attenuation at 9.0 GHz., calculated from standard formulas, is 53.08 dB/cm. The result read from Fig. 3 is 53 dB/cm. Likewise, in the extreme of small conductivity, the attenuation for the case of $\epsilon_r = 2$ is 45 dB/cm; for $\epsilon_r = 4$, 36 dB/cm (some difficulties were encountered in obtaining convergence for this case); for $\epsilon_r = 8$, 25.8 dB/cm; for $\epsilon_r = 16$, 15 dB/cm; and for $\epsilon_r = 32$, 0.146 dB/cm. The latter case differs from the previous ones in that it shows a continuous variation from TEM coaxial line to a *propagating* TM-01 circular waveguide. In this case the dielectric loading is sufficient that a circular waveguide of 7.52-mm diameter is above cutoff at 9 GHz.

Theoretical data of the ratio of TM-01 guide wavelength to the free-space wavelength are given in Fig. 4. In the high conductivity region the relative wavelength approaches 1 (more about this later), while in the low-conductivity region it appears to approach infinity in a logarithmic manner. Note that for the case of $\epsilon_r = 32$ the relative guide wavelength approaches a constant as is expected for a waveguide operating above cutoff.

Fig. 5 gives theoretical data of the real part of the complex characteristic impedance normalized to 50 Ω, and Fig. 6 gives corresponding data for the imaginary component. Note that the normalized absolute value is plotted in Fig. 6 rather than the signed value. The imaginary part is capacitive for the TM mode. The complex characteristic impedance exhibits those general properties that are now expected. That is, in the region of high conductivity the real part approaches a constant and the imaginary part approaches zero; while in the region of low conductivity, the real part approaches zero and the imaginary part approaches a constant, at least for those cases where the TM-01 mode is cutoff. For the case of $\epsilon_r = 32$, the roles are reversed: the real part approaches a constant equal to the characteristic impedance of the propagating waveguide, while the imaginary part approaches zero.

The reader may have noted that the curves thus far do not appear to asymptotically approach expected theoretical values in the limit of large conductivity. This is due to the fact that the conductivity has not been extended to sufficiently large values. Fig. 7 presents representative data of the real part of the characteristic impedance and the relative guide wavelength for conductivities of from 10 to 10^5 for $\epsilon_r = 1$. (The conductivity of copper is 5.7×10^7 mhos/m). We see from Fig. 7 that the relative guide wavelength does indeed approach 1 (the computer value is 0.9969), and the real part of the characteristic impedance is equal to 71.38 Ω at $\sigma = 10^5$ mhos/m. The conventional

theoretical value is given by $59.95*\ln(b/a)$ which yields 71.15 Ω in this case. Thus, there is excellent agreement between the asymptotic values from the computer program and known theoretical values from the literature. One more comparison may be of some interest.

The computer result for attenuation slope for $\sigma = 10^5$ mhos/m is 0.05093 dB/cm. The corresponding result calculated from Moreno's formula [6], allowing for an outer conductor of infinite conductivity, is 0.05046. Again this quite remarkable agreement, together with the previously mentioned results, gives substantial credence to the correctness of all of the data, and in particular to the data on which the design of the experimental coaxial-line attenuator was based.

Practical Design Considerations

The longitudinal section view of the attenuator given in Fig. 1 suggests a number of practical mechanical and electrical considerations. Mechanically, the two halves of the attenuator should be concentric and circular, wall thicknesses should be minimized and items 2 and 7 require a sliding fit. These conditions imply tightly toleranced parts.

The principle electrical considerations are the dimensions of the coaxial lines and the material to be used for item 7. With regard to the latter, the data of Fig. 3 suggests that the material should have a small relative dielectric constant and, in order to have a reasonable attenuation-slope, a conductivity in the vicinity of 10–20 mhos/m. Smaller conductivities would give greater attenuation but would result in impractical characteristic impedances. A search of the technical literature reveals few natural materials having these properties. However, commercial silicon is available with this range of conductivity, although its relative dielectric constant (11.7) is greater than desired. Nevertheless, its availability and purity make it a good candidate. Also in its favor is the fact that the conductivity of doped silicon can now be toleranced to 5 percent, thus assuring good consistency from attenuator to attenuator. Although silicon is not isotropic, its small anisotropy should not noticably effect attenuator performance.

An experimental attenuator was constructed for the frequency band 6–12 GHz. The dimensions of the lossy part of the attenuator were those used for the compilation of the data given in Figs. 3–6. These data gave an overall perspective of the attenuator as a function of center conductor conductivity. However, in order to select an optimum value for the semi-insulator conductivity, design data as a function of frequency were also compiled. Fig. 8 shows a part of the data used to optimize the conductivity. Examination of the data shows that for $\sigma = 11$ the variation is 0.6 dB/cm over the band; while for $\sigma = 12$ the variation is ± 0.45 dB/cm. However, $\sigma = 11$ provides greater attenuation. After due consideration it was decided to use $\sigma = 11$, and a center conductor length of 1.0 cm in the experimental attenuator.

For n-type silicon $\sigma = 11$ corresponds to an impurity concentration of 6×10^{14} donors/cm^3. This is well above

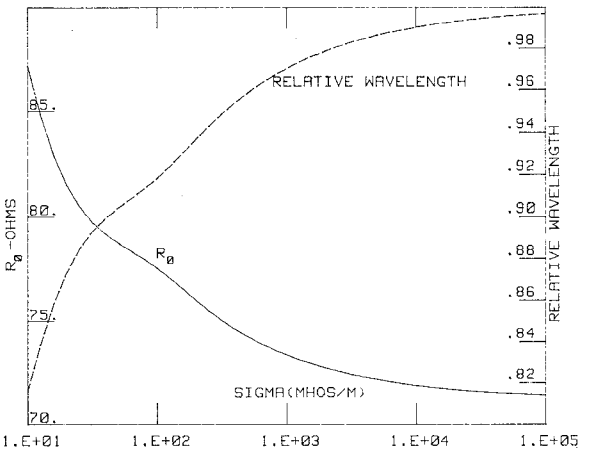

Fig. 7. Normalized guide wavelength and real part characteristic impedance versus conductivity.

the value for intrinsic silicon which is 2×10^5 donors/cm^3 [7]. This is an important practical consideration since it indicates that the temperature dependence of the conductivity will be a 3/2 power relationship rather than exponential [8].

Experimental Results

A photograph of an early experimental coaxial-line attenuator is shown in Fig. 9. Attenuation measurements prior to impedance matching the attenuator are given in Fig. 10 for approximate frequencies 6, 9, and 12 GHz. The curves have been normalized to give 0 dB at the origin. The attenuation at the 0-cm position was less than 0.75 dB across the band. The curves show surprisingly good linearity even for small values of center conductor extension. A closer examination on a more expanded scale showed some convexness, in qualitative agreement with results obtained from computer simulations.

Measured VSWR data are given in Fig. 11 for center-conductor positions of 0, 0.5, and 1 cm. For practical purposes the impedance has converged by 1-cm extension of the center conductor as can be inferred from the data. The measured VSWR differs from the theoretical value for an infinite lossy coaxial line because of the support beads and other junction effects. Consequently, theoretical values cannot be used in the design of a matching network.

Matching

An examination of the attenuator geometry in Fig. 1 shows that impedance matching is best accomplished from the side of the attenuator to which the silicon is attached. On the other side of the attenuator, only impedance steps that are less than 50 Ω are possible. Hence, the matching cannot be expected to work as well. Using measured data of input impedance, a stepped impedance matching network of noncommensurate lines was designed using computer aided methods. Starting with the section adjacent to the silicon, the matching network had line impedances of 99.9, 37.1, 28.2, and 36.1 Ω; and lengths of 2.76, 7.21, 9.24, and 8.21 mm. Discontinuity

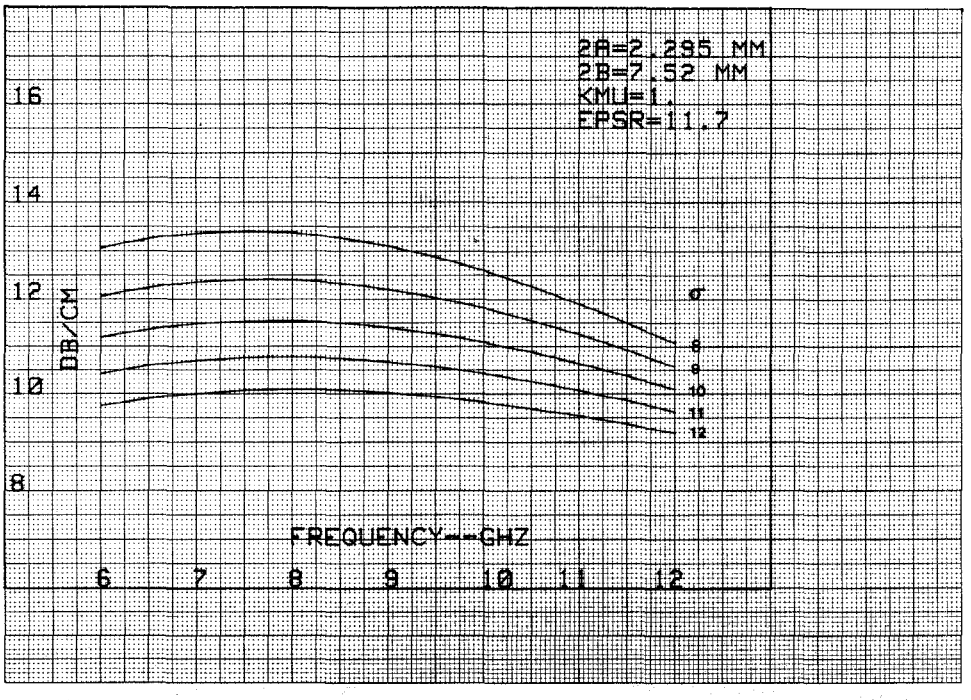

Fig. 8. Theoretical attenuation slope versus frequency.

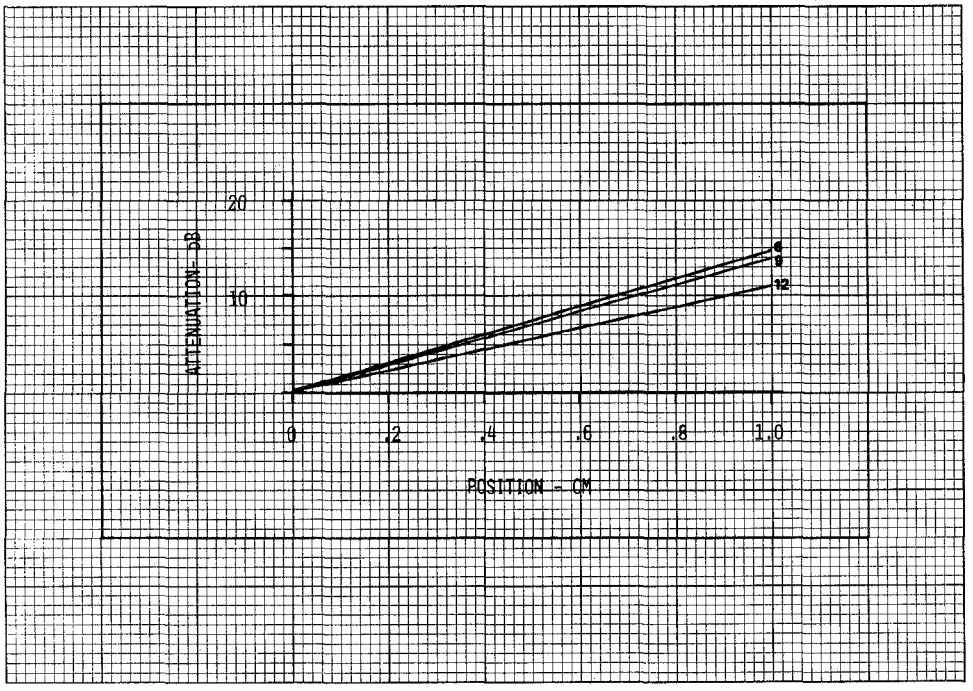

Fig. 9. Photograph of an experimental coaxial variable attenuator.

capacitances at the steps were automatically accounted for in the computer program using Somlo's formula [9]. The matching network was constructed and added to the silicon side of the attenuator. The other side of the attenuator was left unmatched. The measured VSWR for 1-cm extension is also shown in Fig. 11. It is less than 1.55 across the band. On the other hand the VSWR (with the matching network) for 0-cm extension was slightly under 3 at the low end of the band diminishing to slightly above 2 at the high end of the band. A compromise approach to achieve better match is to use silicon having a larger value of conductivity. This would also have the advantage of reducing the frequency dependence, but would give less attenuation per centimeter of center-conductor displacement.

Thermal Considerations

Although silicon has several desirable characteristics, one of its principle disadvantages is its temperature sensitivity. Define the attenuation slope (data of Fig. 8) as A_S. An important figure of merit M_T, on a differential basis, is the change in A_S with temperature. This can be expressed

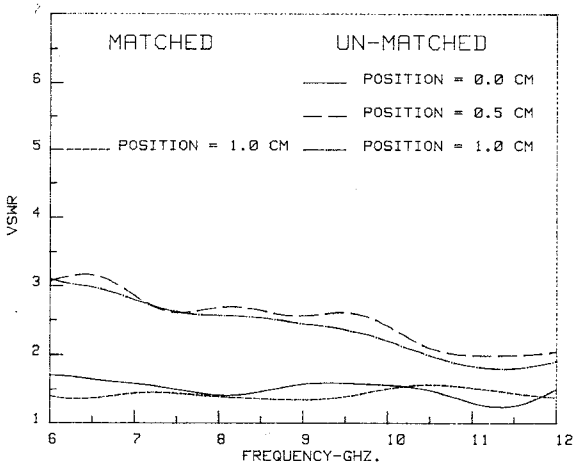

Fig. 10. Measured attenuation versus position (cm) for experimental attenuator.

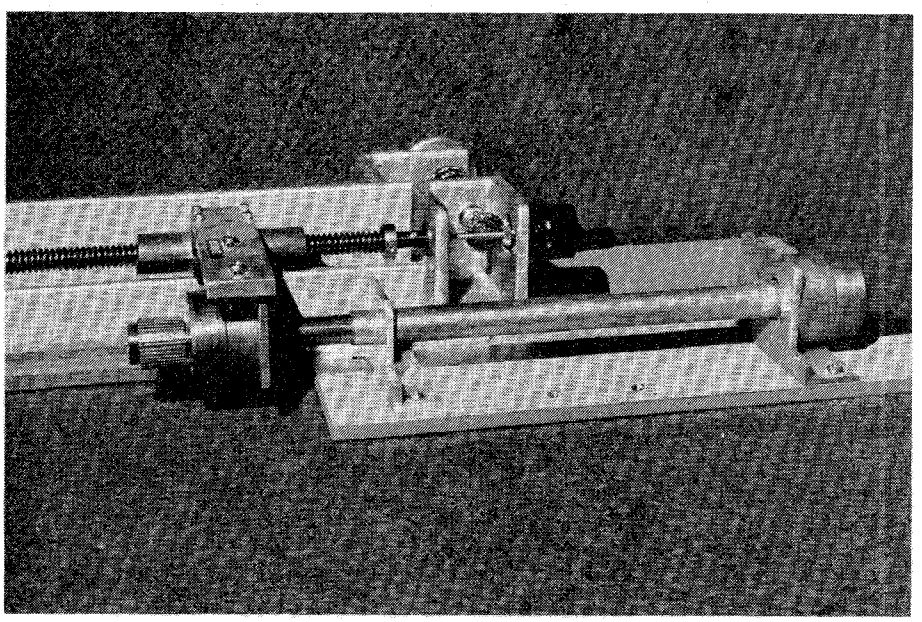

Fig. 11. Measured VSWR versus frequency for matched and unmatched attenuator.

as

$$M_T = \frac{dA_s}{dT} = \frac{dA_s}{d\sigma} \cdot \frac{d\sigma}{d\rho} \cdot \frac{d\rho}{dT} \tag{5}$$

where ρ is the silicon resistivity in $\Omega \cdot$centimeters.

Although frequency dependent, typical values for the component factors in (5) at $\sigma = 11$ and $F = 9.0$ GHz are $dA_s/d\sigma = 0.7$ (dB/cm)/(mhos/m), $d\sigma/d\rho = 1.21$ (mhos/m)/($\Omega \cdot$cm), $d\rho/dT = 0.086$ $\Omega \cdot$cm/°C. [Measured at 25°C] Thus, at 9.0 GHz the quasi-theoretical value is

$$M_T = 0.073 \text{ dB/cm/°C}.$$

Measurements of M_T in a temperature controlled environment agreed reasonably well with theory. These data, either theoretical or experimental, could be used to correct an attenuator readout. For example, an attenuator at 9.0 GHz and 3-cm extension, would require $3 \times 0.07 = 0.21$-dB/°C correction. One possible implementation might be a temperature sensor feeding data to a microprocessor which would compute the correction and reset a digital readout.

Self-heating effects were examined using computer simulation. Conduction, convection and radiation effects were considered, but only conduction was found significant. For silicon bonded to Kovar the theoretical temperature rise for 10 mW of input power was approximately 0.25 °C. For conductors of brass, copper, and Kovar-copper combinations the temperature rises were much less. Thus, self-heating effects for RF levels of 10 to say 50 mW of RF power can be neglected.

Conclusions

Theory, theoretical data and design guidelines were presented for a new continuously variable coaxial-line attenuator. An experimental prototype covering the 6- to

12-GHz band verified the feasibility of the design concept. Performance tradeoffs between frequency flatness, attenuation slope, and impedance matching were discussed. The attenuator's inherent characteristics suggest applications calling for moderate bandwidths up to an octave, attenuation ranges to approximately 60 dB, or possibly greater (limited by the mechanical strength of the semi-insulator), and controlled temperature environments unless compensation is intended.

Appendix

1) Electromagnetic field equations in Region I of Fig. 2:

$$E_z = \frac{B\gamma}{j\omega\epsilon_0}\left[J_0(\gamma r)N_0(\gamma b) - N_0(\gamma r)J_0(\gamma b)\right]\exp(-\Gamma z)$$

$$E_r = \frac{B\Gamma}{j\omega\epsilon_0}\left[J_1(\gamma r)N_0(\gamma b) - N_1(\gamma r)J_0(\gamma b)\right]\exp(-\Gamma z)$$

$$H_\theta = B\left[J_1(\gamma r)N_0(\gamma b) - N_1(\gamma r)J_0(\gamma b)\right]\exp(-\Gamma z)$$

$$B = \frac{I}{2\pi a}\left[J_1(\gamma a)N_0(\gamma b) - N_1(\gamma a)J_0(\gamma b)\right]^{-1}$$

where I is the low-frequency conduction current.

$$\gamma^2 = \Gamma^2 - (j\omega\epsilon_0)(j\omega\mu_0).$$

2) Electromagnetic field equations in Region II of Fig. 2:

$$E_z = \frac{I}{2\pi a}\,\frac{\hat{\gamma}}{\sigma + j\omega\epsilon}\,\frac{J_0(\hat{\gamma}r)}{J_1(\hat{\gamma}a)}\exp(-\Gamma z)$$

$$E_r = \frac{I}{2\pi a}\,\frac{\Gamma}{\sigma + j\omega\epsilon}\,\frac{J_1(\hat{\gamma}r)}{J_1(\hat{\gamma}a)}\exp(-\Gamma z)$$

$$H_\theta = \frac{I}{2\pi a}\,\frac{J_1(\hat{\gamma}r)}{J_1(\hat{\gamma}a)}\exp(-\Gamma z)$$

$$\hat{\gamma}^2 = \Gamma^2 - (\sigma + j\omega\epsilon)(j\omega\mu).$$

Acknowledgment

The author would like to thank B. Benson who first pointed out the suitability of commercial doped silicon, H. Hiner who contributed significantly to the successful hybridization of the silicon center conductor and the coaxial line, R. Jordan and H. Grashof for their critical mechanical design, B. Heinz and S. Lund for thoughtful technical discussions, and B. Raukko and H. Halverson for their support throughout the investigation.

References

[1] J. B. Gunn and C. A. Hogarth, "A novel microwave attenuator using germanium," *J. App. Phys.*, vol. 26, pp. 353–354, 1955.

[2] H. Bacher and J. Ebert, "Linear variable lossy-line attenuator," U. S. Patent 3 237 133, Feb. 27, 1964.

[3] B. O. Weinschel, "Inside-out attenuator for high frequency coaxial-lines," U.S. Patent 3 002 166, Sept. 26, 1961.

[4] D. E. Bergfried, "Variable resistive film attenuator," U.S. Patent 3 786 374, Jan. 15, 1974.

[5] S. A. Schelkunoff, *Electromagnetic Waves*. New York: Van Nostrand, 1943, Ch 12.

[6] T. Moreno, *Microwave Transmission Design Data*. New York: Dover, 1943

[7] A. S. Grove, *Physics and Technology of Semiconductor Devices*. New York: Wiley, 1967

[8] W. M. Bullis *et al.*, "Temperature coefficient of resistivity of silicon and germanium near room temperature," vol. 11, *Solid State Electronics*. New York: Pergamon, 1968.

[9] P. I. Somlo, "The computation of coaxial line step capacitances," *IEEE Trans. Microwave Theory and Tech.*, MTT-15, pp. 48–53; Jan. 1967.